p53 integrates host defense and cell fate during bacterial pneumonia

Jennifer H. Madenspacher,[1] Kathleen M. Azzam,[1] Kymberly M. Gowdy,[1] Kenneth C. Malcolm,[6] Jerry A. Nick,[6] Darlene Dixon,[2,3] Jim J. Aloor,[1] David W. Draper,[1] John J. Guardiola,[1] Maria Shatz,[4] Daniel Menendez,[4] Julie Lowe,[4] Jun Lu,[5] Pierre Bushel,[5] Leping Li,[5] B. Alex Merrick,[3] Michael A. Resnick,[4] and Michael B. Fessler[1]

[1]Laboratory of Respiratory Biology; [2]Cellular and Molecular Pathology Branch, [3]National Toxicology Program; [4]Laboratory of Molecular Genetics; and [5]Biostatistics Branch; National Institute of Environmental Health Sciences, National Institutes of Health, Research Triangle Park, NC 27709
[6]Department of Medicine, National Jewish Health, Denver, CO 80206

Cancer and infection are predominant causes of human mortality and derive, respectively, from inadequate genomic and host defenses against environmental agents. The transcription factor p53 plays a central role in human tumor suppression. Despite its expression in immune cells and broad responsiveness to stressors, it is virtually unknown whether p53 regulates host defense against infection. We report that the lungs of naive $p53^{-/-}$ mice display genome-wide induction of NF-κB response element–enriched proinflammatory genes, suggestive of type 1 immune priming. p53-null and p53 inhibitor–treated mice clear Gram-negative and -positive bacteria more effectively than controls after intrapulmonary infection. This is caused, at least in part, by cytokines produced by an expanded population of apoptosis-resistant, TLR-hyperresponsive alveolar macrophages that enhance airway neutrophilia. $p53^{-/-}$ neutrophils, in turn, display heightened phagocytosis, Nox-dependent oxidant generation, degranulation, and bacterial killing. p53 inhibition boosts bacterial killing by mouse neutrophils and oxidant generation by human neutrophils. Despite enhanced bacterial clearance, infected $p53^{-/-}$ mice suffer increased mortality associated with aggravated lung injury. p53 thus modulates host defense through regulating microbicidal function and fate of phagocytes, revealing a fundamental link between defense of genome and host during environmental insult.

CORRESPONDENCE
Michael B. Fessler:
fesslerm@niehs.nih.gov

Abbreviations used: AEBSF, 4-(2-aminoethyl)benzenesulfonyl fluoride; BALF, bronchoalveolar lavage fluid; ChIP, chromatin immunoprecipitation; i.t., intratracheal(ly); KC, keratinocyte-derived chemokine; NO, nitric oxide; PEM, peritoneal elicited macrophage; PWM, position weight matrix; ROS, reactive oxygen species; WBC, white blood cell.

The tumor suppressor p53 is a transcriptional master regulator that promotes DNA repair, cell cycle arrest, senescence, and apoptosis in response to challenges to genomic integrity, thereby guarding against oncogenesis (Junttila and Evan, 2009; Vousden and Prives, 2009). Maintained at low levels in the steady-state by proteasomal degradation, p53 is rapidly stabilized and activated in response to DNA damage and a variety of other metabolic stressors (Lavin and Gueven, 2006). In addition to classical genotoxic stress (e.g., γ-irradiation), p53 is also responsive to inflammatory stressors such as TNF (Donato and Perez, 1998) and reactive oxygen species (ROS; Lavin and Gueven, 2006; Vousden and Prives, 2009) and is up-regulated at sites of inflammation (Moon et al., 2000; Hofseth et al., 2003).

Recent studies have extended the purview of p53 as a suppressor gene by demonstrating that p53 also regulates inflammation. p53 suppresses NF-κB–dependent cytokine induction (Komarova et al., 2005; Liu et al., 2009; Ak and Levine, 2010). p53 also regulates cell migration through interactions with Rho GTPases (Sablina et al., 2003) and exerts complex effects on oxidant generation, promoting release of mitochondrial ROS during stress-induced apoptosis, but also buffering ROS under more physiological settings through induction of antioxidant genes and repression of inducible nitric oxide (NO) synthase (Polyak et al., 1997; Ambs et al., 1998; Sablina et al., 2005). Cytokine induction, cell migration, and oxidant generation are not only

The Rockefeller University Press $30.00
J. Exp. Med. 2013 Vol. 210 No. 5 891-904
www.jem.org/cgi/doi/10.1084/jem.20121674

The Journal of Experimental Medicine

hallmarks of inflammation, but also pivotal events in host defense. However, very few studies have investigated a possible role for p53 in infection. These investigations have been limited to viral inoculation (Takaoka et al., 2003; Turpin et al., 2005; Muñoz-Fontela et al., 2008), a setting in which cell-intrinsic hallmark functions of p53 established in the tumor suppressor literature (e.g., cell cycle arrest and apoptosis) had also already been established to play a central role in clearance of cells infected with oncogenic and nononcogenic viruses alike.

Host defense against extracellular as well as intracellular pathogens in complex organs such as the lung requires coordinated actions by multiple cell types. Alveolar macrophages, as sentinel cells, play a critical role through both cell-intrinsic antimicrobial functions (e.g., generation of oxidants) and production of cytokines that recruit microbicidal neutrophils (PMNs) into the infected airspace. Ultimately, death of macrophages and PMNs through apoptosis is coupled to their production of oxidants and is critical for successful bacterial clearance (Marriott et al., 2006). Given the importance of these various cellular functions to host defense, we speculated that the ubiquitously expressed tumor suppressor p53 might be positioned to regulate multiple critical checkpoints in the host defense response to extracellular pathogens in vivo.

Here, we show that mice with deletion or inhibition of p53 display enhanced clearance of both Gram-negative and -positive extracellular bacteria after intrapulmonary infection. p53-deficient mice have an expanded population of apoptosis-resistant, TLR-hyperresponsive alveolar macrophages, recruiting increased PMNs into the airspace. $p53^{-/-}$ PMNs, in turn, display coordinate enhancement of a suite of antimicrobial functions. Collectively, these findings suggest that p53 regulates host defense against extracellular pathogens through coordinate control of function and fate of phagocytes in the lung, thus positioning p53 as a fundamental link between defense of the organism and of the genome in the face of environmental insult.

RESULTS

p53 deletion and inhibition enhance clearance of extracellular bacteria during pneumonia

To determine whether p53 regulates antibacterial host defense in the lung, $p53^{-/-}$ and $p53^{+/+}$ mice were inoculated intratracheally (i.t.) with the Gram-negative bacterium *Klebsiella pneumoniae*, and extrapulmonary bacterial dissemination was monitored by blood culture. As shown in Fig. 1 A, $p53^{-/-}$ mice had significantly lower organism burden in blood than WT counterparts 24 and 48 h after lung infection. Similar findings were noted after lung infection with the Gram-positive bacterium *Streptococcus pneumoniae* (Fig. 1 B). In parallel with the blood culture findings, $p53^{-/-}$ mice had a nearly 2-log reduction in splenic bacteria 48 h after i.t. infection with *K. pneumoniae* (Fig. 1 C), consistent with reduced bacteremic seeding. WT mice pretreated with a single i.p. dose of the p53 inhibitor pifithrin-α (PFTα; Komarov et al., 1999) also had lower splenic *K. pneumoniae* CFUs than vehicle-treated counterparts, suggesting that pharmacologic antagonism of p53 is also effective at reducing pathogen burden in the setting of pneumonia. PFTα-treated $p53^{-/-}$ mice had higher splenic bacterial CFUs than vehicle-treated $p53^{-/-}$ mice, consistent with some off-target effects of the inhibitor; however, direct treatment of *K. pneumoniae* with PFTα in vitro revealed no effects on bacterial growth (not depicted). Confirming that bacterial clearance is indeed enhanced in the inoculated lung itself in the setting of p53 deficiency, both $p53^{-/-}$ mice and PFTα-treated $p53^{+/+}$ mice had significantly reduced organism burden in lung homogenates 24 h after i.t. *K. pneumoniae* (Fig. 1 D). Collectively, these findings indicate that reduction of p53, either genetically or by inhibition, enhances pathogen clearance in the setting of bacterial pneumonia.

p53 deficiency enhances neutrophil recruitment to the infected lung

Recruitment of circulating PMNs to the infected lung is critical for successful clearance of bacteria. $p53^{-/-}$ mice recruited more leukocytes to the airspace than WT counterparts in the setting of infections with both *K. pneumoniae* and *S. pneumoniae*, reflecting increases in both PMNs and macrophages (Fig. 2, A and B). PFTα-treated WT mice similarly recruited

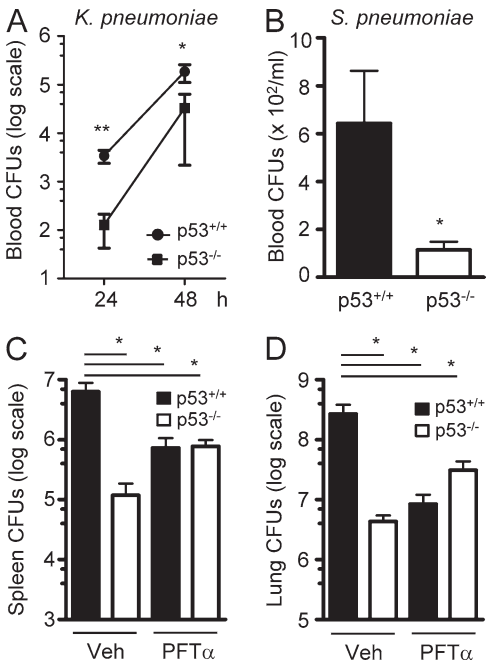

Figure 1. p53-deficient mice display enhanced bacterial clearance. (A) Quantitative blood cultures in $p53^{+/+}$ and $p53^{-/-}$ mice 24 and 48 h after i.t. inoculation with *K. pneumoniae* (n = 9–10/genotype/time point; representative of two independent experiments). (B) Quantitative blood cultures 24 h after i.t. inoculation with *S. pneumoniae* (n = 9–10/genotype; representative of two independent experiments). (C) Splenic homogenate cultures 48 h after i.t. *K. pneumoniae* in mice pretreated with either PFTα or vehicle (Veh; n = 12–14/condition; representative of three independent experiments). (D) Lung homogenate cultures from mice treated as in C. Data are representative of three independent experiments. Data are mean ± SEM. *, $P < 0.05$; **, $P < 0.01$.

increased PMNs to the airspace after *K. pneumoniae* infection (Fig. 2 C). In response to inhalation of LPS, the canonical ligand for TLR4 and the major immunostimulatory glycolipid of the Gram-negative bacterial cell wall, $p53^{-/-}$ mice also recruited increased PMNs to the airspace in a sustained manner over 48 h after exposure (Fig. 2 D).

Abundance of PMNs in the airway is regulated as a balance between PMN recruitment from the bloodstream on the one hand and PMN apoptosis and clearance on the other. As p53 is a proapoptotic factor and is expressed by PMNs (Hsieh et al., 1997), we queried whether neutrophilia in the infected $p53^{-/-}$ airspace might in part stem from reduced PMN apoptosis. Intraalveolar PMNs, however, displayed equivalent rates of apoptosis in the $p53^{+/+}$ and $p53^{-/-}$ airway both in the naive state and 24 h after i.t. *K. pneumoniae* (Fig. 2 E), as indicated by flow cytometry of FLIVO, a poly-caspase reporter (Merrick et al., 2011). This finding suggests that the airway neutrophilia in infected $p53^{-/-}$ mice is not driven by reduced PMN apoptosis. Naive $p53^{-/-}$ mice also had normal numbers of circulating PMNs and other leukocyte subtypes (Table 1), thus ruling out steady-state peripheral neutrophilia, as might conceivably occur through an effect of p53 on cell cycle in the bone marrow (Leonova et al., 2010), as an explanation for increased numbers of PMNs recruited to the airspace of infected $p53^{-/-}$ mice.

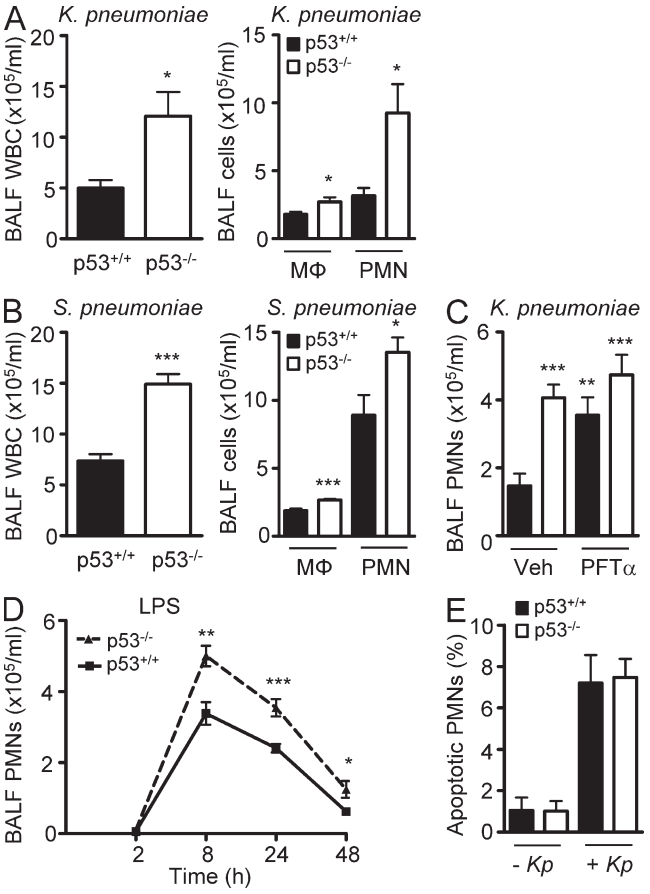

Figure 2. p53-deficient mice recruit increased PMNs and macrophages to the infected lung. (A and B) BALF total leukocyte (WBC), macrophage (MΦ), and PMN counts 24 h after i.t. infection with *K. pneumoniae* (A) and *S. pneumoniae* (B; $n = 10$/genotype; representative of two independent experiments/pathogen). (C) BALF PMNs 24 h after i.t. *K. pneumoniae* in $p53^{+/+}$ and $p53^{-/-}$ mice pretreated with PFTα or vehicle (Veh; $n = 9$/condition; representative of two independent experiments). (D) BALF PMNs in $p53^{+/+}$ and $p53^{-/-}$ mice at various time points after inhalation of LPS ($n = 5$–13/genotype/time point; representative of three independent experiments). (E) Frequency of apoptosis in BALF PMNs was quantified in unexposed (−*Kp*) and i.t. *K. pneumoniae*–exposed (+*Kp*) mice by flow cytometric measurement of caspase activation (FLIVO) in $Gr1^+$ BALF cells ($n = 6$, −*Kp*; $n = 11$, +*Kp*; representative of two independent experiments). Data are mean ± SEM. *, $P < 0.05$; **, $P \leq 0.005$; ***, $P < 0.005$.

p53 deletion leads to genome-wide proinflammatory gene induction in the lung

Given that p53 is a transcription factor with both activation and repression activity, we performed gene expression profiling on noninfected $p53^{-/-}$ and $p53^{+/+}$ mouse lung to screen for possible mechanisms underlying the enhanced inflammatory response in the p53-null lung. 258 genes were significantly ($P < 0.01$) up ($n = 186$)- or down-regulated ($n = 72$) >2.0-fold in $p53^{-/-}$ as compared with $p53^{+/+}$ lung (Table S1).

Remarkably, gene ontology analysis (DAVID tool, http://david.abcc.ncifcrf.gov/tools.jsp) revealed striking enrichment of immune response genes (false discovery rate = 7.6×10^{-22}; 152 regulated genes in immune gene ontology categories) in the naive $p53^{-/-}$ lung, including a wide variety of proinflammatory genes (cytokines, cytokine receptors, integrins, and prooxidant enzymes) that were up-regulated compared with WT lungs (Fig. 3 A). Given this, we analyzed the promoter regions of regulated genes to identify potential NF-κB–binding sites using the Genomatix MatInspector tool (Cartharius et al., 2005). 252 (97.7%) of the genes differentially expressed in the $p53^{-/-}$ lung were noted to possess high-confidence–predicted NF-κB–binding sites (5.0 ± 0.2 [mean ± SEM] sites per gene) in their promoters (Tables S2 and S3), suggesting that they may be NF-κB target genes. To more stringently test the in silico enrichment of NF-κB motifs in the promoter regions of genes up-regulated in the $p53^{-/-}$ lung, we performed a comprehensive, unbiased analysis. To do this, we first identified promoter sequences (1 kb) for the up-regulated genes in

Table 1. Peripheral WBC count and differential in naive $p53^{+/+}$ and $p53^{-/-}$ mice

Cell type	Cell count	
	$p53^{+/+}$	$p53^{-/-}$
	$\times 10^3/\mu l$	$\times 10^3/\mu l$
WBCs	7.0 ± 2.34	7.1 ± 2.78
Neutrophils	0.68 ± 0.26	1.03 ± 0.81
Monocytes	0.24 ± 0.11	0.22 ± 0.11
Lymphocytes	6.03 ± 2.41	5.72 ± 2.66
Eosinophils	0.14 ± 0.11	0.18 ± 0.10

Values are mean ± SD. Monocyte data were derived from $n = 5$/genotype; for all others, $n = 10$. All inter-genotype comparisons are P = NS.

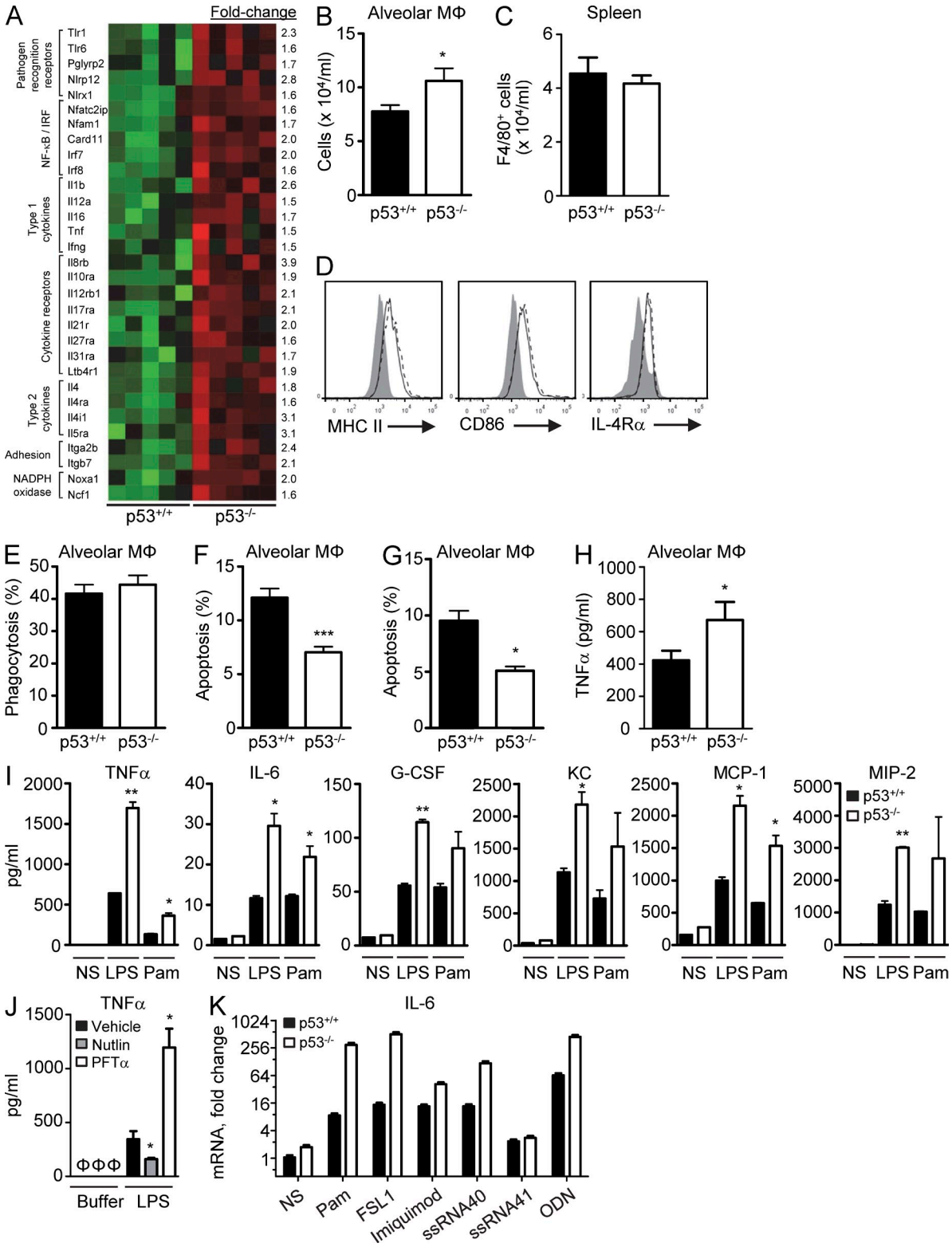

Figure 3. Inflammatory priming of the p53-null lung and macrophages. (A) Proinflammatory genes up-regulated in naive $p53^{-/-}$ as compared with $p53^{+/+}$ lung. Columns represent microarray data from separate mice. Mean fold change is shown at right and functional categories at left. Data are representative of one experiment involving $n = 5$ mice/genotype. (B) Alveolar macrophage (MΦ) number in naive $p53^{+/+}$ and $p53^{-/-}$ mice ($n = 14–15$/genotype; representative of three independent experiments). (C) Number of $F4/80^+$ macrophages in spleen of naive $p53^{+/+}$ and $p53^{-/-}$ mice ($n = 3$/genotype; representative of two independent experiments). (D) Representative flow cytometry histograms of MHC class II, CD86, and IL-4Rα on alveolar macrophages

$p53^{-/-}$ lung; 287 were identified, accounting for alternative transcription start sites. Next, 10 control promoter sequences were selected randomly from the mouse genome for each of the 287 promoters, matched for G-C content. We then used GADEM software (Li, 2009) to scan both sets of sequences with each of the position weight matrices (PWMs) in the JASPAR (Sandelin et al., 2004), TRANSFAC (Knüppel et al., 1994), and UniPROBE (Newburger and Bulyk, 2009) databases. For each PWM, we counted the number of sequences containing at least one predicted site for the PWM. The significance of enrichment in the p53 gene set compared with the control set was then assessed using a one-sided Fisher's exact test. NF-κB was indeed identified as the top-ranked, enriched motif in the $p53^{-/-}$ gene set over the control set by both the TRANSFAC ($P = 2.3 \times 10^{-4}$) and JASPAR ($P = 5.5 \times 10^{-4}$) models. Moreover, of the 87 NF-κB motifs identified by both databases, 80 were confirmed to correspond to unique genes, thereby further indicating that the NF-κB motif enrichment is not caused by over-representation of NF-κB sites in genes possessing multiple predicted promoters.

16S rDNA analysis of aseptically harvested lung indicated no evidence for increased microbial colonization of naive $p53^{-/-}$ lungs compared with $p53^{+/+}$ lungs (not depicted). Moreover, bronchoalveolar lavage fluid (BALF) levels of a wide panel of cytokines and chemokines (MIP-2, IL-6, IL-17, keratinocyte-derived chemokine [KC], MCP-1, and TNF) were equivalent between naive $p53^{+/+}$ and $p53^{-/-}$ mice (not depicted), arguing against overt inflammation in naive $p53^{-/-}$ lungs. Although the significance of the altered global gene expression in the naive $p53^{-/-}$ lung was not fully clear, it was reminiscent of the transcriptional priming for secondary pro-inflammatory exposures that has been described with IFN-γ (El Chartouni and Rehli, 2010) and suggested to us the possibility that the $p53^{-/-}$ lung may be poised for a more robust immune response during infection. We thus more closely examined immune cell populations in the $p53^{-/-}$ lung.

Expansion of TLR-hyperresponsive macrophages in the $p53^{-/-}$ lung

Alveolar macrophages play a critical role in pulmonary host defense against *S. pneumoniae* and other extracellular pathogens (Dockrell et al., 2003). Naive $p53^{-/-}$ mice had higher numbers of alveolar macrophages than $p53^{+/+}$ mice (Fig. 3 B), whereas alveolar PMNs and lung parenchymal dendritic cells, $CD4^+$ T cells, $CD8^+$ T cells, and B cells were comparable in number with WT mice (not depicted), consistent with a macrophage-specific expansion of lung-resident leukocytes. In contrast, $p53^{-/-}$ mice had normal numbers of splenic $F4/80^+$ macrophages (Fig. 3 C), ruling out a global expansion of tissue macrophages, and normal numbers of blood monocytes (Table 1), ruling out systemic monocytosis.

$p53^{-/-}$ alveolar macrophages appeared normal in terms of development and maturity, expressing WT levels of cell surface MHC class II, CD86, and IL-4Rα (Fig. 3 D) and also displaying normal morphology (not depicted) and phagocytic function (Fig. 3 E). However, $p53^{-/-}$ alveolar macrophages had a lower rate of constitutive in vivo apoptosis than $p53^{+/+}$ counterparts, as indicated by both a poly-caspase activity reporter (Fig. 3 F) and a caspase-3/7–specific activity reporter (Fig. 3 G).

Notably, $p53^{-/-}$ alveolar macrophages produced higher levels of TNF than $p53^{+/+}$ counterparts in response to LPS exposure (Fig. 3 H). $p53^{-/-}$ peritoneal elicited macrophages (PEMs) also produced higher levels of cytokines than WT controls in response to both LPS and Pam3CSK4, a synthetic TLR2 ligand used to model Gram-positive bacterial lipoproteins (Fig. 3 I). WT PEMs pretreated with PFTα also induced elevated TNF in response to LPS, whereas pretreatment with the p53 activator nutlin-3a diminished TNF induction (Fig. 3 J). $p53^{-/-}$ bone marrow–derived macrophages also induced higher IL-6 than WT counterparts in response to a yet wider panel of pathogen-associated molecular patterns, including stimuli for TLR2 (Pam3CSK4 and FSL1), TLR7 (imiquimod), TLR8 (ssRNA40), and TLR9 (ODN; Fig. 3 K). Collectively, these findings suggest that p53 deletion coordinately enhances the number and global innate immune responsiveness of macrophages in the lung.

Enhanced induction of NF-κB–dependent cytokines in the infected $p53^{-/-}$ lung

Compared with WT counterparts, alveolar macrophages in $p53^{-/-}$ mice also had a reduced rate of programmed cell death, as well as higher cell surface display of the co-stimulatory protein CD86 24 h after i.t. inoculation with *K. pneumoniae* (Fig. 4, A and B), together suggesting that they may sustain higher viability and activation status during lung infection.

($CD11c^+autofluorescence^{hi}$) of naive $p53^{+/+}$ and $p53^{-/-}$ mice. Shaded trace is isotype control, solid line is $p53^{+/+}$, and dashed line is $p53^{-/-}$. Data are representative of two independent experiments. (E) Ex vivo phagocytosis of *E. coli* bioparticles by naive $p53^{+/+}$ and $p53^{-/-}$ alveolar macrophages ($n = 5$/genotype; representative of two independent experiments). (F and G) Apoptosis rates of alveolar macrophages from naive $p53^{+/+}$ and $p53^{-/-}$ mice, as quantified by flow cytometry of poly-caspase activation (FLIVO; F) or caspase-3/7 activation (FLICA; G; $n = 6$/genotype for both assays; representative of two independent experiments). (H) Alveolar macrophages (>98%) were lavaged from $p53^{+/+}$ and $p53^{-/-}$ mice 1 h after LPS inhalation and resuspended in culture. TNF production into media was evaluated 6 h later by ELISA ($n = 8$–10/genotype; representative of two independent experiments). (I) PEMs from $p53^{+/+}$ and $p53^{-/-}$ mice were exposed to LPS and Pam3CSK4 (Pam) and conditioned media assayed by multiplex assay for the indicated cytokines ($n = 4$/genotype; data representative of two independent experiments). (J) $p53^{+/+}$ PEMs were pretreated with vehicle, 10 µM nutlin-3, or 40 µM PFTα, exposed to buffer or LPS, and then assayed by ELISA for TNF release ($n = 2$–3/condition; representative of two independent experiments). Φ, not detected. (K) Bone marrow–derived $p53^{+/+}$ and $p53^{-/-}$ macrophages were either left nonstimulated (NS) or exposed (24 h) to TLR ligands (1 µg/ml Pam3CSK4, 100 ng/ml FSL1, 10 µg/ml imiquimod, 1 µg/ml ssRNA40 [ssRNA41 is negative control for ssRNA40], and 5 µM ODN2395), after which normalized IL-6 mRNA expression was quantified by quantitative PCR. Data shown (log_2 scale) are representative of four independent experiments. Data are mean ± SEM. *, $P \leq 0.05$; **, $P < 0.01$; ***, $P < 0.001$.

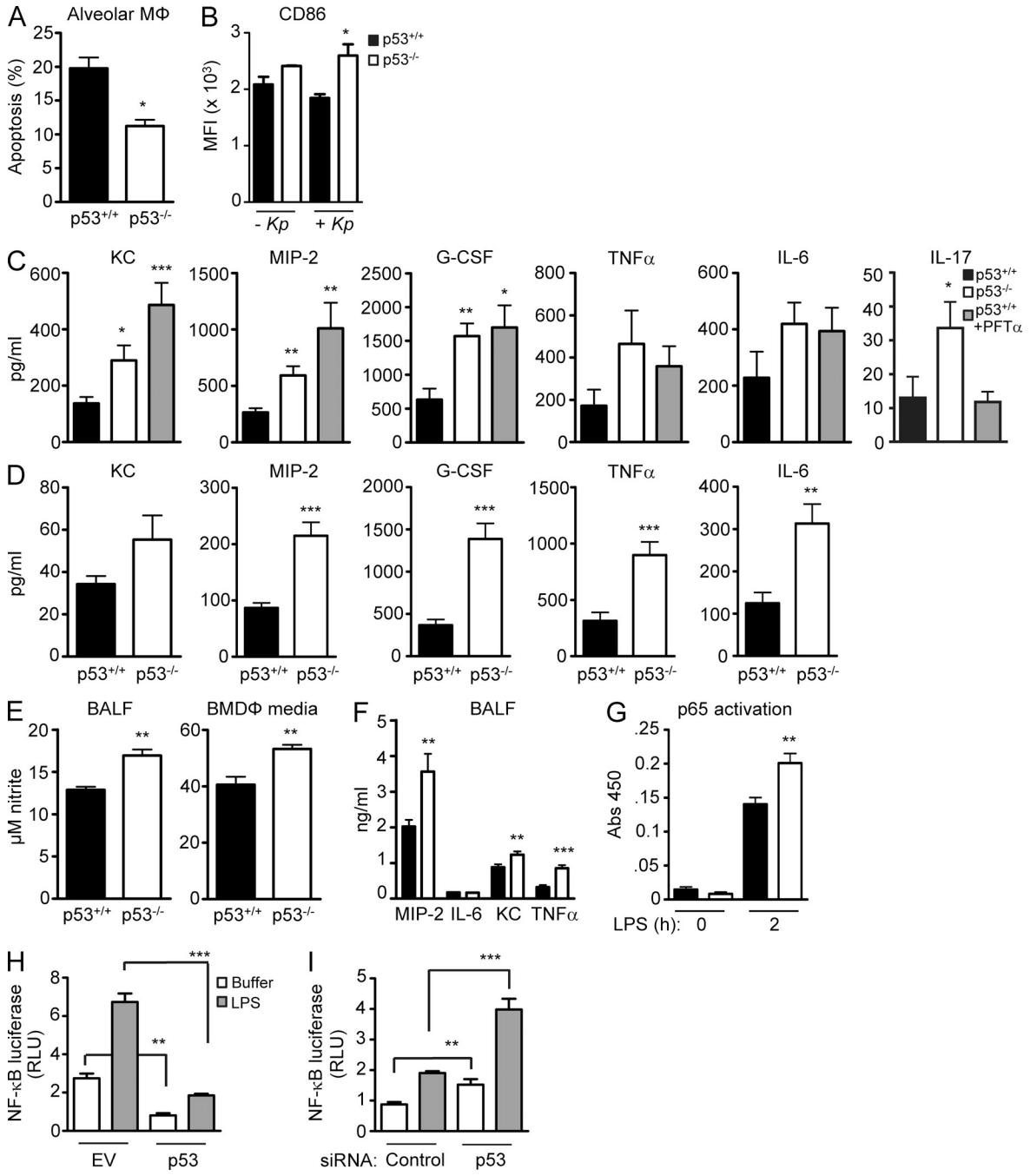

Figure 4. Increased induction of NF-κB–dependent cytokines in the infected p53-null lung. (A) Programmed cell death (flow cytometric measurement of caspase activity [FLIVO]) of alveolar macrophages (MΦ) in $p53^{+/+}$ and $p53^{-/-}$ mice 24 h after i.t. *K. pneumoniae* (n = 11/genotype; representative of three independent experiments). (B) CD86 surface display by flow cytometry on alveolar macrophages of unexposed (−*Kp*) and i.t. *K. pneumoniae*–exposed (+*Kp*) $p53^{+/+}$ and $p53^{-/-}$ mice (representative of three experiments involving n = 9/genotype). (C and D) BALF cytokines 24 h after i.t. *K. pneumoniae* (C) or *S. pneumoniae* (D) in $p53^{+/+}$, $p53^{-/-}$, or PFTα-treated $p53^{+/+}$ mice (n = 10/condition; representative of two independent experiments/pathogen). (E) BALF total nitrite, an indicator of NO, in $p53^{+/+}$ and $p53^{-/-}$ mice 48 h after i.t. *K. pneumoniae* (left; n = 5/genotype) and in conditioned media of $p53^{+/+}$ and $p53^{-/-}$ bone marrow–derived macrophages 24 h after treatment with 50 U/ml IFN-γ and 100 ng/ml LPS (right; n = 6/genotype). Data are representative of two to three independent experiments. (F) BALF cytokines in $p53^{+/+}$ and $p53^{-/-}$ mice 2 h after LPS inhalation (n = 10/genotype; representative of two independent experiments). (G) p65 NF-κB activation in lung homogenates of $p53^{+/+}$ and $p53^{-/-}$ mice 2 h after LPS inhalation (n = 6–10/genotype/time point; representative of two independent experiments). (H) NF-κB luciferase activity (RLU, relative light units) in buffer- or LPS-exposed CD14-MD2-TLR4-HEK293 cells transfected with empty vector (EV) or p53 (representative of two independent experiments). (I) NF-κB luciferase activity in buffer- or LPS-exposed CD14-MD2-TLR4-HEK293 cells transfected with p53 plus either negative control siRNA or p53 siRNA (representative of two independent experiments). Data are mean ± SEM. *, $P < 0.05$; **, $P < 0.01$; ***, $P < 0.001$.

Given the enhanced ex vivo cytokine induction by $p53^{-/-}$ macrophages and increased number of viable and activated alveolar macrophages in the infected $p53^{-/-}$ lung, we examined BALF cytokine levels during infection. BALF of $p53^{-/-}$ mice infected with either *K. pneumoniae* or *S. pneumoniae* also contained elevated levels of a wide range of cytokines and chemokines of established importance to PMN recruitment (Fig. 4, C and D). In the case of *K. pneumoniae*, treatment of WT mice with PFTα produced a similar increase over vehicle treatment for all analytes other than IL-17 (Fig. 4 C). BALF of *K. pneumoniae*–infected $p53^{-/-}$ mice also contained elevated NO (Fig. 4 E), an oxidant integral to host defense against extracellular bacteria (Tsai et al., 1997). In support of $p53^{-/-}$ alveolar macrophages contributing to this finding, $p53^{-/-}$ bone marrow–derived macrophages displayed higher NO production after LPS/IFN-γ treatment than WT counterparts. To confirm the effect of p53 deletion on airspace cytokine induction in a more acute and simplified model, mice were exposed to inhaled LPS. $p53^{-/-}$ mice had higher BALF TNF, KC, and MIP-2 than WT counterparts 2 h after LPS inhalation, a time point which precedes significant influx of PMNs to the lung (not depicted), whereas IL-6 was equivalent to WT (Fig. 4 F).

NF-κB plays a critical role in induction of cytokines by lung-resident cells, PMN recruitment to the airspace, and bacterial clearance during pneumonia (Quinton et al., 2007) and is reportedly suppressed by p53 (Komarova et al., 2005; Ak and Levine, 2010). Thus, we next quantified NF-κB DNA binding in the nuclear fraction of lung parenchyma after LPS inhalation. LPS-induced p65 NF-κB DNA binding activity was higher in $p53^{-/-}$ than WT lung after LPS (Fig. 4 G). In further support of a suppressive effect of p53 on NF-κB transcriptional activity, overexpression of p53 attenuated both basal and LPS-induced NF-κB luciferase activity in TLR4-CD14-MD2-HEK293 cells, whereas p53 silencing enhanced basal and LPS-induced NF-κB luciferase (Fig. 4, H and I). Collectively, these findings suggest that the enhanced neutrophilia in the infected $p53^{-/-}$ airspace may stem from enhanced cytokine/chemokine induction in the airway that in turn derives, at least in part, from enhanced NF-κB activation in lung-resident cells.

p53 regulates migration of PMNs to the lung in vivo

p53 is also expressed by both PMNs and the lung structural cells (i.e., epithelium and endothelium) that PMNs interact with during their complex integrated passage from blood to airspace. To test whether PMNs display a migratory advantage to the airspace in $p53^{-/-}$ mice, CXCL1/KC was instilled i.t. in $p53^{+/+}$ and $p53^{-/-}$ mice, and PMN influx into the airway was quantified. As shown in Fig. 5 A, significantly more PMNs accumulated in the $p53^{-/-}$ airway than in WT controls 4 h after KC. BALF KC was equivalent in $p53^{+/+}$ and $p53^{-/-}$ mice at this time point, suggesting equal chemokine bioavailability, and BALF MIP-2 was also similar between genotypes, whereas G-CSF, TNF, and IL-6 were lower in the $p53^{-/-}$ airway after i.t. KC (not depicted). Collectively, these findings indicate that (a) more PMNs enter $p53^{-/-}$ than WT airways even in the setting of an equal inoculum of chemokines, (b) enhanced PMN influx into the $p53^{-/-}$ airway in response to KC is not explained by more robust secondary induction of chemokines, and (c) the effect of p53 on airway cytokine induction is stimulus dependent.

p53-deficient PMNs display enhanced antimicrobial functions

Although enhanced airway neutrophilia and NO might suffice to explain the enhanced bacterial clearance in the $p53^{-/-}$ lung, we next sought to determine whether p53 deletion also alters PMN functions involved in phagocytic killing. As shown in Fig. 5 B, $p53^{-/-}$ peritoneal elicited PMNs were indeed observed to phagocytose bacterial bioparticles more effectively than WT counterparts. To model PMN phagocytic killing at inflammatory foci in vivo (Ledford et al., 2007), *K. pneumoniae* was next injected i.p. into $p53^{+/+}$ and $p53^{-/-}$ mice after thioglycollate eliciting PMNs to the peritoneum; peritoneal PMNs were then harvested 30 min after peritoneal infection and assayed for intracellular bacterial killing during a time course ex vivo. As shown in Fig. 5 C, $p53^{-/-}$ PMNs displayed enhanced killing of *K. pneumoniae*. Ex vivo treatment of the harvested peritoneal PMNs with BAY 11-7082, an NF-κB inhibitor, did not significantly alter intracellular killing by PMNs of either genotype (not depicted), arguing against an important role for PMN NF-κB in intracellular bacterial killing in this system.

Killing of bacteria in the PMN phagosome is thought to derive from NADPH oxidase 2 (Nox2)–derived superoxide (O_2^-) as well as granule proteases such as elastase, although the major role of oxidants may be to license proteases by promoting their release from proteoglycan matrix (Reeves et al., 2002). $p53^{-/-}$ peritoneal elicited PMNs produced higher levels of O_2^- than WT PMNs after stimulation with either the Nox2 activator PMA or the bacterial tripeptide formylated-Met-Leu-Phe (fMLF; Fig. 5 D). Consistent with this increased O_2^- deriving from Nox2, O_2^- induction by both stimuli was abolished in PMNs of both genotypes pretreated with the Nox2 inhibitor diphenyleneiodonium (Fig. 5 D), as well as in peritoneal PMNs harvested from $gp91^{phox-/-}$ (i.e., Nox2 deficient) mice (not depicted). $p53^{-/-}$ PMNs displayed increased expression of gp91phox and the cytosolic Nox2-activating protein p47phox (Fig. 5 E), consistent with upregulation of the Nox2 complex. In contrast, p67phox was not differentially expressed.

Consistent with *p40phox/ncf4*, a positive regulator of Nox2, being a direct suppression target of p53, p53 chromatin immunoprecipitation (ChIP) in RAW 264.7 macrophages pulled down a sequence from the p40phox promoter in a manner that was enhanced by treatment with the p53 activator, nutlin-3 (Fig. 5 F). Indeed, in support of the possibility that p53 may directly regulate expression of multiple mouse Nox2 complex genes through transcriptional repression, promoter analysis revealed putative functional p53 response elements not only in p40phox/*Ncf4* but also in gp91phox/*Nox2*, p47phox/*Ncf1*, p22phox/*Cyba*, and *Noxa1* (Table S4). In contrast, no

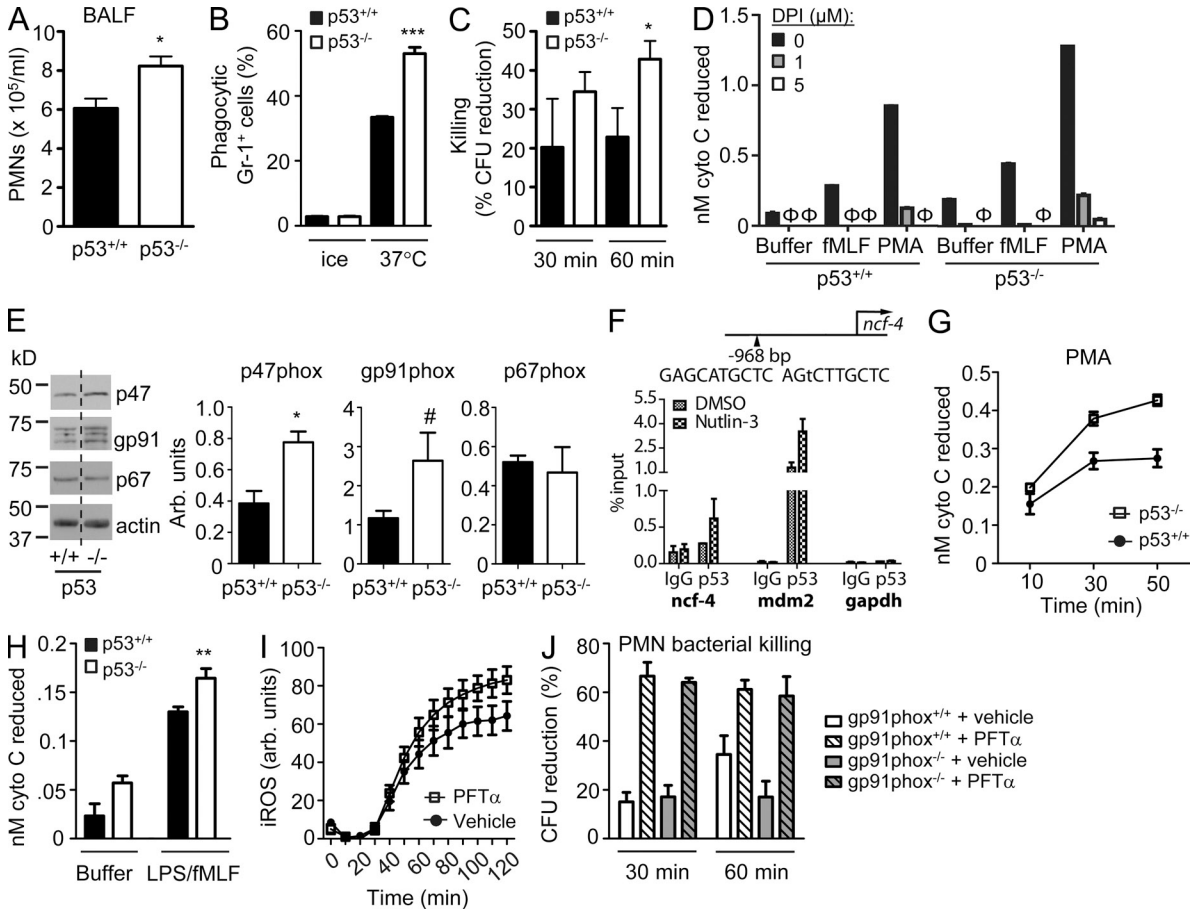

Figure 5. Enhanced microbicidal functions of p53-null PMNs. (A) BALF PMN count in $p53^{+/+}$ and $p53^{-/-}$ mice 4 h after i.t. inoculation with 0.5 μg KC (n = 11/genotype; representative of two independent experiments; *, $P < 0.05$). (B) Phagocytosis of *E. coli* bioparticles by $p53^{+/+}$ and $p53^{-/-}$ peritoneal elicited PMNs (n = 4–6 mice/condition; represents two independent experiments; ***, $P < 0.001$). (C) Intracellular killing by peritoneal PMNs from $p53^{+/+}$ and $p53^{-/-}$ mice exposed to *K. pneumoniae* in vivo (n = 10–12/genotype/time point; represents three independent experiments; *, $P < 0.05$). (D) Superoxide anion generation, as measured by cytochrome *c* reduction, in buffer-, fMLF-, or PMA-treated peritoneal PMNs preincubated with a range of diphenyleneiodonium (DPI). Data represent two to three independent experiments. Φ, not detected. (E) Immunoblots of $p47^{phox}$, $gp91^{phox}$, $p67^{phox}$, and β-actin in mouse PMN lysates. The dashed line demarcates bands that have been juxtaposed from nonadjacent locations on the gel image. Actin-normalized densitometry from n = 3–4 mice/genotype is shown at right. *, $P < 0.05$; #, $P = 0.07$. (F) RAW 264.7 macrophages were exposed (for 16 h) to nutlin-3 or vehicle and then processed for ChIP of p53 (or isotype IgG control). A schematic is shown of a predicted p53-binding sequence in the promoter of ncf4. The promoter regions of ncf4, mdm2 (an established p53 target), and GAPDH (a non-p53 target) were amplified from the precipitates and are plotted as percent input. Data are representative of two independent experiments. (G and H) Superoxide anion generation in $p53^{+/+}$ and $p53^{-/-}$ bone marrow–derived PMNs exposed to PMA (G) or to buffer or 100 ng/ml LPS (30 min) followed by 20 μM fMLF (10 min; H). Data are representative of two independent experiments. **, $P < 0.01$. (I) Intracellular ROS (iROS) generation induced by *K. pneumoniae* in human PMNs (10:1 *Kp*/PMN) pretreated with vehicle or PFTα. $P < 0.0001$ for PFTα vs. vehicle (area under the curve analysis of four experiments). (J) PMN intracellular killing of *K. pneumoniae* was measured as in C, except that $gp91^{phox+/+}$ and $gp91^{phox-/-}$ mice were used that had been injected i.p. with either vehicle or 2.2 mg/kg PFTα at −1 h. Data are mean ± SEM and are representative of two independent experiments (n = 4–5/genotype/time point). $P < 0.001$ for PFTα effect at both time points; P = NS for interaction by genotype (ANOVA).

predicted functional p53 motif was found in the promoter of p67phox/*Ncf2*, consistent with our finding of unchanged expression of p67phox in $p53^{-/-}$ PMNs. *Ncf1* (1.50-fold), *Ncf4* (1.82-fold), and *Noxa1* (2.0-fold) were also significantly upregulated in naive $p53^{-/-}$ as compared with $p53^{+/+}$ lung by microarray analysis, suggesting that constitutive repression of Nox2 complex genes may also occur in the lung.

Increased O_2^- production in response to both PMA and LPS/fMLF was also observed in PMNs isolated from bone marrow of naive $p53^{-/-}$ mice (Fig. 5, G and H). PFTα-treated primary human PMNs also produced higher levels of intracellular ROS than vehicle-treated controls after exposure to *K. pneumoniae* (Fig. 5 I). To test whether the enhanced intracellular killing of p53-deficient PMNs in fact derives from increased O_2^-, the *K. pneumoniae* killing assay was next performed in $gp91^{phox+/+}$ and $gp91^{phox-/-}$ mice pretreated systemically with a single dose of either vehicle or PFTα. Remarkably, as shown in Fig. 5 J (open and hatched open bars), PMNs harvested from $gp91^{phox+/+}$ mice that had been treated systemically with a single dose of PFTα displayed approximately

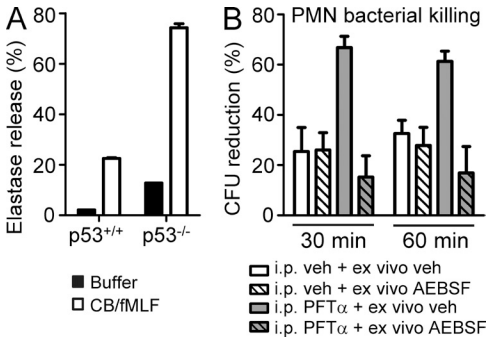

Figure 6. Enhanced killing capacity of p53-inhibited PMNs derives from serine protease activity. (A) Bone marrow PMNs from $p53^{+/+}$ and $p53^{-/-}$ mice were treated with buffer or 5 µg/ml cytochalasin B (for 5 min) followed by 5 µM fMLF (for 20 min); elastase activity released into media was measured by substrate assay and indexed to whole cell elastase activity (percent release). Data are representative of three independent experiments. (B) PMN intracellular killing assay of *K. pneumoniae* was evaluated as in Fig. 5, except that peritoneal PMNs were harvested from i.p. vehicle- versus PFTα-pretreated WT mice and then treated ex vivo (for 30 min) with either 500 µM AEBSF or vehicle (veh) before a killing time course at 37°C. Data are mean ± SEM and represent n = 6–7/condition over two independent experiments. $P < 0.05$ for i.p. PFTα + ex vivo vehicle versus i.p. vehicle + ex vivo vehicle at both time points; $P < 0.001$ for i.p. PFTα + ex vivo vehicle versus i.p. PFTα + ex vivo AEBSF for both time points (ANOVA with Bonferroni post-test).

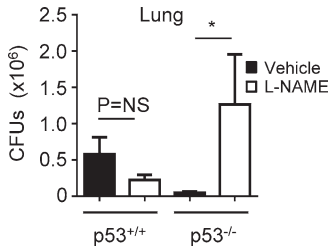

Figure 7. Inhibition of NO synthesis impairs bacterial clearance in the p53-null lung. $p53^{+/+}$ and $p53^{-/-}$ mice were pretreated (−1 h) with either 40 mg/kg L-NAME or vehicle i.p. and then infected in the lungs with 2,000 CFU *K. pneumoniae*. After 24 h, lung CFUs were quantified. Data are mean ± SEM and represent n = 8–9/condition over two independent experiments. *, $P < 0.05$.

fourfold enhanced intracellular bacterial killing. Of note, however, PFTα treatment enhanced bacterial killing by $gp91^{phox-/-}$ PMNs comparably with its effect in $gp91^{phox+/+}$ PMNs. This suggests that increased Nox2 function does not, at least by itself, underlie the enhanced bacterial killing phenotype of p53-deficient PMNs.

Pursuing the protease arm of PMN microbicidal function, we next tested the capacity of PMNs to release elastase by degranulation. Unlike the alternate PMN azurophilic granule serine protease cathepsin G, elastase has a proven role in PMN killing of *K. pneumoniae* (Belaaouaj et al., 1998). $p53^{-/-}$ PMNs indeed released significantly higher elastase activity than WT counterparts upon ex vivo treatment with the azurophilic granule–releasing dual stimulus, cytochalasin B/fMLF (Fig. 6 A). This suggested the possibility that the killing advantage of p53-deficient PMNs might stem from enhanced proteolytic activity. To test this hypothesis, we repeated the PMN intracellular killing assay in i.p. vehicle- and PFTα-treated WT mice, but this time incubated PMNs harvested from the peritonea of both treatment groups with either the cell-permeant general serine protease inhibitor 4-(2-aminoethyl)benzenesulfonyl fluoride (AEBSF) or vehicle (Standish and Weiser, 2009). AEBSF abolished the killing advantage of PMNs from PFTα-treated mice (Fig. 6 B), thereby suggesting that the enhanced killing phenotype of p53-deficient PMNs derives from enhanced serine protease activity.

Several cell types in the lung, in addition to recruited PMNs, are capable of producing NO. NO plays an important role in pulmonary host defense against several types of bacteria, including *K. pneumoniae* (Tsai et al., 1997). Given our finding of increased BALF NO in infected $p53^{-/-}$ mice, we thus questioned whether NO might also contribute to the enhanced clearance of *K. pneumoniae* from the $p53^{-/-}$ lung. To address this, $p53^{+/+}$ and $p53^{-/-}$ mice were treated with either L-NAME (a NO synthase inhibitor) or vehicle and then infected with *K. pneumoniae* for 24 h. As is shown in Fig. 7, L-NAME had no significant effect on clearance of *K. pneumoniae* from $p53^{+/+}$ lungs but dramatically impaired bacterial clearance from $p53^{-/-}$ lungs. This finding suggests that NO plays an important role in the enhanced antibacterial host defense of the $p53^{-/-}$ lung.

$p53^{-/-}$ mice have reduced survival and aggravated lung injury during pneumonia

PMN recruitment to the lung is required for successful host defense, but overexuberant inflammation can harm the host through bystander lung injury. We and others have reported various gene-deleted mouse strains that suffer increased mortality during bacterial pneumonia despite neutrophilia-enhanced pathogen clearance (Li et al., 2009; Draper et al., 2010). Notably, we found that $p53^{-/-}$ mice have lower survival than WT mice after i.t. *K. pneumoniae* (Fig. 8 A). In support of exacerbated lung injury contributing to this outcome, infected $p53^{-/-}$ mice had increased BALF protein (Fig. 8 B), a marker of pulmonary microvascular injury. Moreover, histopathologic analysis of *K. pneumoniae*–infected lungs confirmed significantly increased perivascular neutrophilic inflammation and edema in $p53^{-/-}$ mice 72 h after infection (Fig. 8, C and D).

DISCUSSION

p53 has been extensively studied as a tumor suppressor and more recently shown to be an inflammation suppressor. In the present study, we extend the domain of this master regulatory transcription factor to that of suppression of the host defense response, showing that p53-deficient mice have enhanced clearance of bacterial pneumonia associated with coordinate disinhibition of macrophage and PMN function. We propose that enhanced activation of NF-κB and induction of cytokines in the infected p53-null lung, originating at least in part from an expanded, TLR-hyperresponsive alveolar macrophage population, further augments recruitment of p53-null

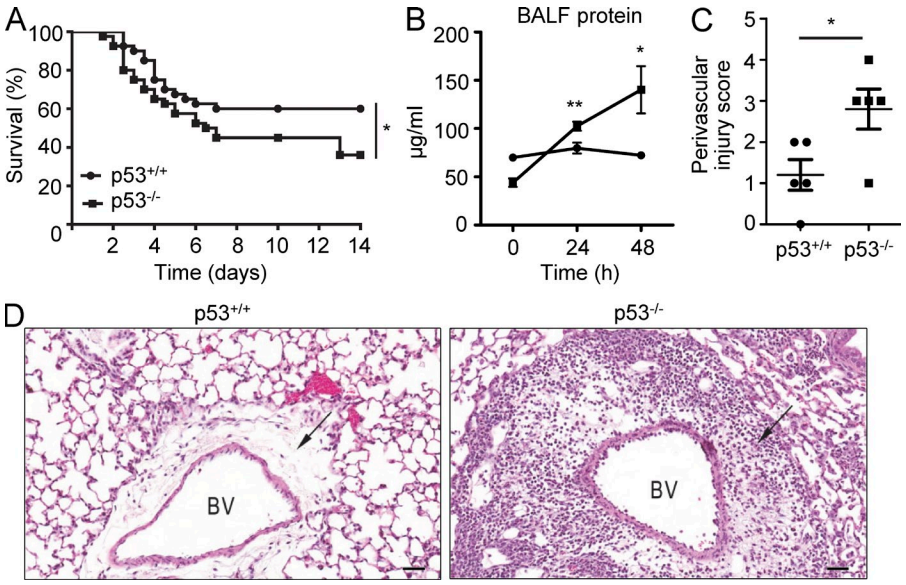

Figure 8. Enhanced mortality and lung injury in infected p53-null mice. (A) Survival of $p53^{+/+}$ and $p53^{-/-}$ mice after i.t. infection with *K. pneumoniae* (n = 30/genotype, representative of three independent experiments). (B) BALF protein of $p53^{+/+}$ and $p53^{-/-}$ mice 0, 24, and 48 h after i.t. *K. pneumoniae* (n = 5–9/genotype/time point; representing two independent experiments; mean ± SEM). (C) Lung perivascular injury (cellular infiltration and edema) was scored by a blinded pathologist 72 h after i.t. *K. pneumoniae* (n = 5/genotype). (D) Representative lung sections (H&E) from analysis in C showing blood vessels (BV), including the tunica adventitia (arrows) of $p53^{+/+}$ and $p53^{-/-}$ mice 72 h after i.t. *K. pneumoniae*. Note increased neutrophilic infiltrates and edema in tunica adventitia of the $p53^{-/-}$ specimen. Bars, 50 µm. *, $P \leq 0.05$; **, $P < 0.01$.

PMNs to the alveolus beyond a migratory advantage they already display in response to alveolar chemokines. $p53^{-/-}$ PMNs, in turn, display coordinate enhancement of a suite of antimicrobial functions, including phagocytosis, bacterial killing, oxidant generation, and granule release. That said, our data do not exclude possible important host defense roles for p53 in nonhematopoietic cells in the lung, such as alveolar epithelial cells. However, in the end, reminiscent of the case for some other gene deletions (e.g., *Abcg1* and *Pten* [Li et al., 2009; Draper et al., 2010]), enhanced pathogen clearance in the p53-null mouse is associated with worsened survival. p53's integrated role may thus be to serve as a beneficial brake on the lung's response to infection. We provide correlative data suggesting that $p53^{-/-}$ mice may suffer lower survival as the result of lung injury from an overexuberant immune response; however, it is very possible that p53 deletion may engender additional maladaptive responses that compromise survival.

We speculate that the p53-null lung is poised for a more robust host defense response at least in part through genome-wide effects of NF-κB disinhibition. Our finding of an NF-κB response element–enriched transcriptional signature of inflammation in the naive p53-null lung is reminiscent of a recent study showing that p53 inhibition and TNF treatment elicit strikingly similar NF-κB target gene–enriched transcriptional profiles in LNCaP prostate cancer cells (Komarova et al., 2005). We are unaware, however, of any previous report that p53 deletion induces inflammatory gene programs in vivo in the steady-state. Of note, NF-κB can be activated by both ROS and DNA damage, and it has been reported that $p53^{-/-}$ mice have increased DNA damage in multiple tissues caused by increased ROS (Sablina et al., 2005). It is thus interesting to speculate that the genomic signature of the $p53^{-/-}$ lung in our study may in part stem from oxidative stress and that p53 may thus exert coordinate control over cancer and inflammation through regulation of ROS.

Alveolar macrophages were also increased in number in the naive $p53^{-/-}$ lung and displayed a reduced rate of constitutive apoptosis, consistent with a report that p53 promotes apoptosis of macrophages in other settings (Mercer et al., 2005). Given the equivalent expression (<1.5-fold difference) of monocyte/macrophage-attracting chemokines (CCL1, -2, -3, -4, -5, -7, -8, and -12) in naive $p53^{-/-}$ and $p53^{+/+}$ lungs (unpublished data) and the normal number of circulating monocytes in $p53^{-/-}$ mice, we speculate that the increase in alveolar macrophages stems, at least in part, from reduced local apoptosis, rather than increased trafficking to the lung. p53 has also been reported to suppress macrophage proliferation (Merched et al., 2003). Although we were unable to detect the proliferation marker PCNA in naive alveolar macrophages by either immunoblotting or flow cytometry, bone marrow–derived $p53^{-/-}$ macrophages expressed significantly increased PCNA compared with WT counterparts (unpublished data), suggesting that increased local proliferation may also possibly contribute to increased numbers of alveolar macrophages in the $p53^{-/-}$ lung. However, of interest, our finding of a normal number of splenic macrophages in $p53^{-/-}$ mice suggests that this regulatory effect of p53 on steady-state macrophage populations is tissue selective.

Macrophage apoptosis has been reported to be essential not only for resolution of inflammation but also for successful clearance of *S. pneumoniae* (Dockrell et al., 2003; Marriott et al., 2006). Although the reduced apoptosis of alveolar macrophages in the infected $p53^{-/-}$ lung was not associated with impaired microbial clearance, it is possible that sustained macrophage survival in the $p53^{-/-}$ lung nonetheless contributed to amplifying inflammation and organ injury. A prior report that $p53^{-/-}$ macrophages have defective efferocytosis (Komarova et al., 2005) may offer a unifying mechanism for the $p53^{-/-}$ pneumonia phenotype in our study, as efferocytosis impairs bacterial clearance (Medeiros et al., 2009) and represses inflammation (Huynh et al., 2002). Suggesting cell type specificity,

and consistent with a prior report that Bcl-2 family members play a dominant role in regulation of PMN apoptosis (Dzhagalov et al., 2007), PMN apoptosis was unaltered in vivo in infected $p53^{-/-}$ mice.

We report a critical role for the molecule NO in the enhanced bacterial clearance phenotype of the $p53^{-/-}$ lung. Treatment of $p53^{-/-}$ mice with the NO synthase inhibitor L-NAME markedly impaired clearance of *K. pneumoniae* from the lung, whereas no such effect was seen in $p53^{+/+}$ mice. In addition to PMNs, several lung-resident cell types have the capacity to generate NO. In support of the possibility that alveolar macrophages may be the responsible cell type, we found that $p53^{-/-}$ bone marrow–derived macrophages produce elevated NO after in vitro stimulation. Thus, in addition to contributing to increased PMN influx during pneumonia via augmented cytokine induction, $p53^{-/-}$ alveolar macrophages may also contribute more directly to microbial killing through enhanced NO generation. Further studies are warranted to identify whether additional cell types in the $p53^{-/-}$ lung, including the alveolar epithelium, may also contribute to increased bacterial killing through augmented NO generation.

Our findings indicate a novel role for p53 as a master regulator of multiple hallmark host defense functions of the PMN. Remarkably, a single systemic injection of PFTα enhanced bacterial killing by PMNs and bacterial clearance in vivo, suggesting potential for p53 inhibitors as immunostimulatory adjuvants. Our use of bone marrow–purified PMNs suggests that at least some of these p53-regulated functions (e.g., O_2^- and elastase release) are, moreover, cell autonomous. Although others have demonstrated that p53 buffers ROS through induction of antioxidants (Sablina et al., 2005), we are unaware of prior reports that p53 regulates Nox-dependent generation of O_2^- in any cell type. p53 may modulate Nox function at least in part through directly repressing Nox2 complex genes. However, the finding that PFTα enhances PMN bacterial killing comparably in Nox2-sufficient and -deficient PMNs indicates that enhanced O_2^- does not, at least in isolation, explain the enhanced killing conferred by p53 deficiency. $p53^{-/-}$ PMNs also released increased elastase, a critical executor protease of bacterial killing (Belaaouaj et al., 1998). We provide evidence that the killing advantage of p53-deficient PMNs derives from enhanced serine protease and, likely, elastase activity. As PMN elastase has been implicated in a wide array of lung disorders and shown to induce p53-dependent lung epithelial apoptosis (Suzuki et al., 2009), we speculate that p53 may represent an under-recognized central regulator of lung disease.

p53 in the lung is indeed broadly responsive to environmental stressors. Diesel exhaust, silica, and cigarette smoke all activate p53 in macrophages and/or other lung cell types (Wang et al., 2005; Yun et al., 2009; Damico et al., 2011), suggesting that these exposures may alter host defense functions at least in part through p53. p53 is also up-regulated in the alveolar epithelium in chronic obstructive lung disease (Siganaki et al., 2010). As small molecule p53 agonists are under development for human cancer therapy, future studies are urgently needed to define the effects of pharmacologic activation of p53 on the human innate immune response in vivo. Moreover, as chemotherapeutics already in wide clinical use as well as radiation therapy also activate p53, it is incumbent to determine whether these agents modify innate immunity and pneumonia risk in cancer patients via effects on p53. Finally, studies are warranted to determine whether genetic polymorphisms leading to hypofunction of the p53 pathway are associated with increased risk for lung injury and/or mortality during human pneumonia.

The recent recognition that bacteria and their products induce DNA damage and compromise DNA repair (Koturbash et al., 2009; Güngör et al., 2010) and, conversely, that DNA repair enzymes regulate the innate immune response (Haskó et al., 2002) has suggested that defense of the host and of the genome may be intrinsically interconnected to a degree not previously appreciated. We speculate that p53 may be centrally positioned to integrate these two fundamental responses to the environment and that this carries wide-ranging implications for human disease.

MATERIALS AND METHODS

Reagents. *Escherichia coli* 0111:B4 LPS, penicillin, streptomycin, and BAY 11-7082 were purchased from Sigma-Aldrich. *K. pneumoniae* 43816 (serotype 2), *S. pneumoniae* (serotype 3), DMEM, and FBS were purchased from the American Type Culture Collection. The Bio-Rad Laboratories protein assay was used. KC was purchased from R&D Systems. L-NAME was purchased from Cayman Chemical.

Mice. C57BL/6, B6.129S2-Trp53^{tm1Tyj}/J (backcrossed at least 7 times to C57BL/6), and B6.129S-Cybb^{tm1Din}/J male mice (backcrossed >10 times to C57BL/6), 7–10-wk-old and weighing 18–22 g, were used and were obtained from the Jackson Laboratory. B6.129S-Cybb^{tm1Din}/J mice were provided by J.-S. Hong (National Institute of Environmental Health Sciences [NIEHS], Research Triangle Park, NC). All experiments were performed in accordance with the Animal Welfare Act and the U.S. Public Health Service Policy on Humane Care and Use of Laboratory Animals after review by the Animal Care and Use Committee of the NIEHS.

In vivo exposures. Exposure to 300 μg/ml of aerosolized LPS (30 min) was performed as previously described (Draper et al., 2010). 0.5 μg/60 μl KC, 150–2,000 CFU/50 μl *K. pneumoniae*, and 2×10^5 CFU/50 μl *S. pneumoniae* were delivered to lung by oropharyngeal aspiration during isoflurane anesthesia. In some experiments, 2.2 mg/kg PFTα or vehicle was injected i.p. 1 h preceding other exposures, as previously reported (Komarov et al., 1999).

BALF collection and analysis. BALF was collected immediately after sacrifice, and cells counts were performed as previously described (Draper et al., 2010). Total protein was quantified by the method of Bradford.

PMN and macrophage harvests and culture. Mature mouse bone marrow PMNs were isolated from mouse femurs and tibias by discontinuous Percoll gradient centrifugation as previously reported (Draper et al., 2010). Mouse bone marrow–derived macrophages were prepared and cultured in DMEM containing 10% (vol/vol) FBS and 10% (vol/vol) L cell–conditioned medium as a source of M-CSF for 5 d as previously described (Doan et al., 2004). Peritoneal exudate macrophages were harvested by peritoneal lavage 96 h after i.p. injection of 2 ml of 4% Brewer's thioglycollate. Alveolar macrophages were harvested by airway lavage of naive mice, followed by enrichment by adherence on plastic. Human PMNs were purified from peripheral blood of healthy human donors by discontinuous plasma-Percoll

centrifugation, in accordance with a National Jewish Hospital Institutional Review Board–approved protocol, as previously described (Fessler et al., 2004).

Bactericidal assays. Lung, spleen, and liver were excised after sacrifice and homogenized in PBS, and serial dilutions were plated on tryptic soy agar for bacterial quantification 16 h later, as previously described (Draper et al., 2010). Blood was collected from right ventricle and similarly plated after serial dilution. Intracellular killing capacity of PMNs against i.p. injected *K. pneumoniae* was quantified as reported previously (Ledford et al., 2007). In brief, mice (pretreated at −1 h with 2.2 mg/kg PFTα/vehicle i.p. or left untreated) received 2.5 ml of 4% thioglycollate i.p., followed 4 h later by 10^8 CFUs of *K. pneumoniae* i.p. Peritoneal leukocytes were then collected 30 min later by lavage (HBSS with 100 µg/ml gentamicin), washed, and then retreated, as appropriate, with either vehicle or 40 µM PFTα. In a subset of experiments, the cells were also treated ex vivo with 500 µM AEBSF or vehicle. Morphological analysis of cytospins confirmed that $p53^{+/+}$ and $p53^{-/-}$ peritoneal lavages, as well as post-i.p. vehicle and post-i.p. PFTα peritoneal lavages, contained equal absolute and relative (>80% of lavage cells) PMNs. 10^6 cells were incubated (37°C) for varying durations, followed by lysis (0.1% Triton X-100) for intracellular CFU quantification by plating.

ROS and elastase assays. For analysis of superoxide release, PMNs were exposed either to 1 µg/ml PMA (for 10 min) or to 100 ng/ml LPS (for 30 min) followed by 10 µM fMLF (for 10 min). Superoxide release was then quantified by cytochrome *c* reduction assay, as previously reported (Fessler et al., 2004). Intracellular ROS in *K. pneumoniae*–exposed PMNs (10:1 *Kp*/PMN) were quantified with CM-H2DCFDA (Life Technologies) fluorescence according to the manufacturer's instructions. For analysis of elastase activity, PMNs in phenol red–free RPMI were treated with 5 µg/ml cytochalasin B (for 5 min) followed by 5 µM fMLF (for 20 min), after which cell-free supernatants were incubated (at 37°C for 60 min) with 0.4 mM elastase substrate I (EMD) and read at 410 nm. Supernatants were indexed to whole cell lysate elastase activity to determine percent release of cellular elastase activity.

Cytokine analysis. Cytokines were quantified by multiplex assay (Bio-Plex; Bio-Rad Laboratories) or by ELISA (eBioscience).

NF-κB activity assays. Activation of the p65 component of NF-κB in the nuclear fraction from lung homogenates (Nuclear Extract kit; Active Motif) was quantified by use of a sandwich ELISA (p65 TransAM kit; Active Motif) after normalizing nuclear protein input (Bradford assay). 9×10^4 CD14-MD2-HEK293 cells (InvivoGen) were stably transfected with pcDNA3.1-TLR4 and then transiently transfected with DharmaFECT (Thermo Fisher Scientific) in 24-well poly-lysine–coated plates with 200 ng/well NF-κB luciferase and 50 ng/well Renilla luciferase along with 10 ng/well of either pcDNA3 flag p53 or pcDNA3 (vector control) and 40 nM p53 siRNA (ON-TARGETplus SMARTpool siRNA J-003329-14; Thermo Fisher Scientific) or scrambled siRNA (ON-TARGETplus Non-targeting Pool D-001810; Thermo Fisher Scientific). Cells were then exposed to 200 ng/ml *E. coli* 0111:B4 LPS and harvested after 6 h, and normalized NF-κB luciferase activity was measured by luminometry (Synergy 2, BioTek).

Western blotting. PMNs were lysed in 1× Laemmli/20 mM DTT, and nuclear fractions from mouse lung parenchyma were isolated using the Nuclear Extract kit (Active Motif) according to the manufacturer's instructions. Protein was resolved by 10% SDS-PAGE, transferred to nitrocellulose (Bio-Rad Laboratories), and probed with primary antibodies (all used at 1:1,000). Rabbit anti-p47phox and rabbit anti-p67phox were obtained from EMD Millipore. Rabbit anti-gp91phox was obtained from Abcam. Rabbit anti–β-actin was obtained from Cell Signaling Technology. Goat anti-p53 and rabbit anti-HDAC1 were obtained from Santa Cruz Biotechnology, Inc. Membranes were then washed in Tween Tris-buffered saline (TTBS) and exposed for 60 min to 1:5,000 species-specific HRP-conjugated secondary antibody (GE Healthcare) in 5% milk/TTBS. After further washes, signal was detected with ECL Western Blot Detection Reagents (GE Healthcare), followed by film exposure (GE Healthcare).

RNA isolation and quantitative PCR. RNA was isolated by the RNeasy kit (QIAGEN). cDNAs were generated from 1.5 µg of purified RNA using TaqMan reverse transcription reagents from Applied Biosystems. Real-time PCR was performed in triplicate with TaqMan PCR Mix (Applied Biosystems) in the HT7900 ABI sequence Detection System (Applied Biosystems). Predesigned primers were purchased from Applied Biosystems (information available upon request). Gene expression was normalized to β-2-microglobulin (B2M) gene, and expression levels in untreated control samples were set as one.

Microarray and bioinformatic analysis. Gene expression analysis was conducted using Agilent Whole Mouse Genome 4 × 44 multiplex format oligo arrays (014868; Agilent Technologies) according to the Agilent one-color microarray-based gene expression analysis protocol. Starting with 500 ng of total RNA, Cy3-labeled cRNA was produced according to the manufacturer's protocol. For each sample, 1.65 µg of Cy3-labeled cRNAs was fragmented and hybridized (17 h). Slides were washed and then scanned with an Agilent Technologies scanner. Data were obtained using the Agilent Technologies Feature Extraction software (version 9.5), using the one-color defaults for all parameters. The Agilent Technologies Feature Extraction software performed error modeling, adjusting for additive and multiplicative noise. The resulting data were processed using the Rosetta Resolver system (version 7.2; Rosetta Biosoftware). ANOVA was performed followed by the Benjamini Hochberg false discovery rate multiple test correction. Next, a post-hoc analysis (Tukey-Kramer) was used to perform pairwise comparisons of the group means of the treatment groups to determine which specific pairs were statistically different. The microarray data have been deposited in the NCBI Gene Expression Omnibus and are accessible through GEO series accession no. GSE38420. Promoter regions (−3000 to 1000 from transcription start site) were evaluated for potential NF-κB–binding sites with the use of MatInspector Release professional 8.0.5 software (Genomatix Software GmbH) using the MatInspector family matrix V$NFKB with 0.85 Optimized matrix threshold. Promoter regions were also analyzed for potential p53-binding sites by first identifying putative sites with the use of p53scan (Smeenk et al., 2008) and then ranking these sites for predicted p53 responsivity using established p53 response element functionality rules (Menendez et al., 2009).

Flow cytometry. Lungs and spleen were digested/disaggregated as previously reported (Draper et al., 2012). Anti–Gr-1 (FITC), -F4/80 (PE or APC), -CD11c (PE-Cy5), -CD8a (APC), -CD45R/B220 (APC), and -CD86 (APC) and isotype control antibodies were purchased from BioLegend. Anti-CD4 and -MHCII were purchased from eBioscience. Anti-CD3e (APC) and -CD124/IL-4Ra (PE) were purchased from BD. Cells were stained and fixed with 2% paraformaldehyde/PBS. Flow cytometry was performed using an LSR II (BD) and analyzed using FlowJo (Tree Star) and FCS Express software (De Novo Software).

Assessment of apoptosis. Macrophages and PMNs lavaged from the mouse airway were incubated (for 60 min at 37°C) ex vivo with 1 µl (1:50 DMSO) of either FLIVO, a cell-permeant fluorescent poly-caspase activity reporter, or FLICA, a caspase-3/7–specific activity reporter (ImmunoChemistry Technologies) and then washed twice (0.5% BSA in 1× PBS, pH 7.4). Fluorescence signal was quantified by flow cytometry.

Peripheral blood leukocyte typing and enumeration. The blood samples were analyzed using the HEMAVET 1700 hematology analyzer (Drew Scientific, Inc.). Manual white blood cell (WBC) differential counts were reported, and smear estimates were used to confirm values. Reticulocyte counts were performed using new methylene blue stain and the Miller Disc Method of determination.

Histopathologic analysis. Mice were inoculated i.t. with 2,000 CFUs of *K. pneumoniae* and then sacrificed 3 d later. Lungs were fixed with 4%

paraformaldehyde using a body weight–based volume, embedded in paraffin, sectioned (5 µm), stained with hematoxylin and eosin (H&E), and then semi-quantitatively scored by a pathologist blinded to animal genotype. A scoring system which grades (scale 0–4) the degree of perivascular edema and cellular infiltration (primarily PMNs in this study) in both perivascular and alveolar regions was used, as previously reported (Tilley et al., 2007). Slides were scanned using a ScanScope XT Scanner (Aperio Technologies, Inc.). Sections were viewed and images then captured at 10× using ImageScope software version 11.02.716 (Aperio Technologies, Inc.).

ChIP. RAW 264.7 cells were seeded in 150-mm tissue culture dishes and treated with either DMSO or 10 µM Nutlin-3 (for 16 h). ChIP assays were performed as described previously (Valouev et al., 2008). In brief, the cells were cross-linked and sonicated to yield DNA fragments 200–500 bp in size. Chromatin was immunoprecipitated with either a p53 (Santa Cruz Biotechnology, Inc.) or goat-IgG (Santa Cruz Biotechnology, Inc.) antibody using Invitrogen Protein G Dynabeads. The precipitated DNA was purified with QIAquick PCR Purification (QIAGEN) kit and used as template DNA for SYBR Green PCR reactions (Applied Biosystems). The following primers were used: ncf-4 (FP, 5′-CCCTGCCCATTCTCTCTCTC-3′; and RP, 5′-CCACACACTCAAACCAGGTG-3′), mdm2 (FP, 5′-GACGGCTGCGGAAACG-3′; and RP, 5′-CGGAGGAGCTAAGTCCTGACA-3′), and gapdh (FP, 5′-GTGTGGGGGTTTGTTTGTTC-3′; and RP, 5′-GCATAGGGGCTCACCTGTAA-3′).

Statistical analysis. Analysis was performed using GraphPad Software Prism statistical software. Data are represented as mean ± SEM. Two-tailed Student's *t* test was applied for comparisons of two groups and ANOVA for comparisons of more than two groups. Survival was evaluated by log-rank test. For all tests, $P < 0.05$ was considered significant.

Online supplemental material. Table S1, included as a separate Excel file, indicates genes differentially expressed in naive p53-null lung compared with naive WT lung. Table S2, included as a separate Excel file, shows predicted NF-κB–binding sites in genes differentially expressed in naive p53-null lung. Table S3, included as a separate Excel file, shows the number of predicted NF-κB–binding sites per gene among genes more than twofold regulated in the naive p53-null lung. Table S4, included as a separate Excel file, shows predicted functional p53 response elements found in promoters of mouse Nox complex genes. Online supplemental material is available at http://www.jem.org/cgi/content/full/jem.20121674/DC1.

We thank Deborah King for blood cell counting, Jau-Shyong Hong for Cybb$^{-/-}$ mice, Grace Kissling for statistical analysis, David Fargo for bioinformatic assistance, and the National Institute of Environmental Health Sciences (NIEHS) Microarray Core and Flow Cytometry Core.

This research was supported by the Intramural Research Program of the National Institutes of Health NIEHS (Z01 ES102005) and by 1R01HL090991.

The authors have no conflicting financial interests.

Submitted: 25 July 2012
Accepted: 12 April 2013

REFERENCES

Ak, P., and A.J. Levine. 2010. p53 and NF-κB: different strategies for responding to stress lead to a functional antagonism. *FASEB J.* 24:3643–3652. http://dx.doi.org/10.1096/fj.10-160549

Ambs, S., M.O. Ogunfusika, W.G. Merriam, W.P. Bennett, T.R. Billiar, and C.C. Harris. 1998. Up-regulation of inducible nitric oxide synthase expression in cancer-prone p53 knockout mice. *Proc. Natl. Acad. Sci. USA.* 95:8823–8828. http://dx.doi.org/10.1073/pnas.95.15.8823

Belaaouaj, A., R. McCarthy, M. Baumann, Z. Gao, T.J. Ley, S.N. Abraham, and S.D. Shapiro. 1998. Mice lacking neutrophil elastase reveal impaired host defense against gram negative bacterial sepsis. *Nat. Med.* 4:615–618. http://dx.doi.org/10.1038/nm0598-615

Cartharius, K., K. Frech, K. Grote, B. Klocke, M. Haltmeier, A. Klingenhoff, M. Frisch, M. Bayerlein, and T. Werner. 2005. MatInspector and beyond: promoter analysis based on transcription factor binding sites. *Bioinformatics.* 21:2933–2942. http://dx.doi.org/10.1093/bioinformatics/bti473

Damico, R., T. Simms, B.S. Kim, Z. Tekeste, H. Amankwan, M. Damarla, and P.M. Hassoun. 2011. p53 mediates cigarette smoke-induced apoptosis of pulmonary endothelial cells: inhibitory effects of macrophage migration inhibitor factor. *Am. J. Respir. Cell Mol. Biol.* 44:323–332. http://dx.doi.org/10.1165/rcmb.2009-0379OC

Doan, J.E., D.A. Windmiller, and D.W. Riches. 2004. Differential regulation of TNF-R1 signaling: lipid raft dependency of p42mapk/erk2 activation, but not NF-kappaB activation. *J. Immunol.* 172:7654–7660.

Dockrell, D.H., H.M. Marriott, L.R. Prince, V.C. Ridger, P.G. Ince, P.G. Hellewell, and M.K. Whyte. 2003. Alveolar macrophage apoptosis contributes to pneumococcal clearance in a resolving model of pulmonary infection. *J. Immunol.* 171:5380–5388.

Donato, N.J., and M. Perez. 1998. Tumor necrosis factor-induced apoptosis stimulates p53 accumulation and p21WAF1 proteolysis in ME-180 cells. *J. Biol. Chem.* 273:5067–5072. http://dx.doi.org/10.1074/jbc.273.9.5067

Draper, D.W., J.H. Madenspacher, D. Dixon, D.H. King, A.T. Remaley, and M.B. Fessler. 2010. ATP-binding cassette transporter G1 deficiency dysregulates host defense in the lung. *Am. J. Respir. Crit. Care Med.* 182:404–412. http://dx.doi.org/10.1164/rccm.200910-1580OC

Draper, D.W., K.M. Gowdy, J.H. Madenspacher, R.H. Wilson, G.S. Whitehead, H. Nakano, A.R. Pandiri, J.F. Foley, A.T. Remaley, D.N. Cook, and M.B. Fessler. 2012. ATP binding cassette transporter G1 deletion induces IL-17-dependent dysregulation of pulmonary adaptive immunity. *J. Immunol.* 188:5327–5336. http://dx.doi.org/10.4049/jimmunol.1101605

Dzhagalov, I., A. St John, and Y.W. He. 2007. The antiapoptotic protein Mcl-1 is essential for the survival of neutrophils but not macrophages. *Blood.* 109:1620–1626. http://dx.doi.org/10.1182/blood-2006-03-013771

El Chartouni, C., and M. Rehli. 2010. Comprehensive analysis of TLR4-induced transcriptional responses in interleukin 4-primed mouse macrophages. *Immunobiology.* 215:780–787. http://dx.doi.org/10.1016/j.imbio.2010.05.032

Fessler, M.B., P.G. Arndt, S.C. Frasch, J.G. Lieber, C.A. Johnson, R.C. Murphy, J.A. Nick, D.L. Bratton, K.C. Malcolm, and G.S. Worthen. 2004. Lipid rafts regulate lipopolysaccharide-induced activation of Cdc42 and inflammatory functions of the human neutrophil. *J. Biol. Chem.* 279:39989–39998. http://dx.doi.org/10.1074/jbc.M401080200

Güngör, N., A. Haegens, A.M. Knaapen, R.W. Godschalk, R.K. Chiu, E.F. Wouters, and F.J. van Schooten. 2010. Lung inflammation is associated with reduced pulmonary nucleotide excision repair in vivo. *Mutagenesis.* 25:77–82. http://dx.doi.org/10.1093/mutage/gep049

Haskó, G., J.G. Mabley, Z.H. Németh, P. Pacher, E.A. Deitch, and C. Szabó. 2002. Poly(ADP-ribose) polymerase is a regulator of chemokine production: relevance for the pathogenesis of shock and inflammation. *Mol. Med.* 8:283–289.

Hofseth, L.J., S. Saito, S.P. Hussain, M.G. Espey, K.M. Miranda, Y. Araki, C. Jhappan, Y. Higashimoto, P. He, S.P. Linke, et al. 2003. Nitric oxide-induced cellular stress and p53 activation in chronic inflammation. *Proc. Natl. Acad. Sci. USA.* 100:143–148. http://dx.doi.org/10.1073/pnas.0237083100

Hsieh, S.C., M.H. Huang, C.Y. Tsai, Y.Y. Tsai, S.T. Tsai, K.H. Sun, H.S. Yu, S.H. Han, and C.L. Yu. 1997. The expression of genes modulating programmed cell death in normal human polymorphonuclear neutrophils. *Biochem. Biophys. Res. Commun.* 233:700–706. http://dx.doi.org/10.1006/bbrc.1997.6529

Huynh, M.L., V.A. Fadok, and P.M. Henson. 2002. Phosphatidylserine-dependent ingestion of apoptotic cells promotes TGF-beta1 secretion and the resolution of inflammation. *J. Clin. Invest.* 109:41–50.

Junttila, M.R., and G.I. Evan. 2009. p53—a Jack of all trades but master of none. *Nat. Rev. Cancer.* 9:821–829. http://dx.doi.org/10.1038/nrc2728

Knüppel, R., P. Dietze, W. Lehnberg, K. Frech, and E. Wingender. 1994. TRANSFAC retrieval program: a network model database of eukaryotic transcription regulating sequences and proteins. *J. Comput. Biol.* 1:191–198. http://dx.doi.org/10.1089/cmb.1994.1.191

Komarov, P.G., E.A. Komarova, R.V. Kondratov, K. Christov-Tselkov, J.S. Coon, M.V. Chernov, and A.V. Gudkov. 1999. A chemical inhibitor of p53 that protects mice from the side effects of cancer therapy. *Science.* 285:1733–1737. http://dx.doi.org/10.1126/science.285.5434.1733

Komarova, E.A., V. Krivokrysenko, K. Wang, N. Neznanov, M.V. Chernov, P.G. Komarov, M.L. Brennan, T.V. Golovkina, O.W. Rokhlin, D.V. Kuprash, et al. 2005. p53 is a suppressor of inflammatory response in mice. *FASEB J.* 19:1030–1032.

Koturbash, I., J.E. Thomas, O. Kovalchuk, and I. Kovalchuk. 2009. Heat-killed bacteria induce genome instability in mouse small intestine, liver and spleen tissues. *Cell Cycle*. 8:1935–1939. http://dx.doi.org/10.4161/cc.8.12.8797

Lavin, M.F., and N. Gueven. 2006. The complexity of p53 stabilization and activation. *Cell Death Differ.* 13:941–950. http://dx.doi.org/10.1038/sj.cdd.4401925

Ledford, J.G., M. Kovarova, and B.H. Koller. 2007. Impaired host defense in mice lacking ONZIN. *J. Immunol.* 178:5132–5143.

Leonova, K.I., J. Shneyder, M.P. Antoch, I.A. Toshkov, L.R. Novototskaya, P.G. Komarov, E.A. Komarova, and A.V. Gudkov. 2010. A small molecule inhibitor of p53 stimulates amplification of hematopoietic stem cells but does not promote tumor development in mice. *Cell Cycle*. 9:1434–1443. http://dx.doi.org/10.4161/cc.9.7.11508

Li, L. 2009. GADEM: a genetic algorithm guided formation of spaced dyads coupled with an EM algorithm for motif discovery. *J. Comput. Biol.* 16: 317–329. http://dx.doi.org/10.1089/cmb.2008.16TT

Li, Y., Y. Jia, M. Pichavant, F. Loison, B. Sarraj, A. Kasorn, J. You, B.E. Robson, D.T. Umetsu, J.P. Mizgerd, et al. 2009. Targeted deletion of tumor suppressor PTEN augments neutrophil function and enhances host defense in neutropenia-associated pneumonia. *Blood*. 113:4930–4941. http://dx.doi.org/10.1182/blood-2008-06-161414

Liu, G., Y.J. Park, Y. Tsuruta, E. Lorne, and E. Abraham. 2009. p53 Attenuates lipopolysaccharide-induced NF-kappaB activation and acute lung injury. *J. Immunol.* 182:5063–5071. http://dx.doi.org/10.4049/jimmunol.0803526

Marriott, H.M., P.G. Hellewell, S.S. Cross, P.G. Ince, M.K. Whyte, and D.H. Dockrell. 2006. Decreased alveolar macrophage apoptosis is associated with increased pulmonary inflammation in a murine model of pneumococcal pneumonia. *J. Immunol.* 177:6480–6488.

Medeiros, A.I., C.H. Serezani, S.P. Lee, and M. Peters-Golden. 2009. Efferocytosis impairs pulmonary macrophage and lung antibacterial function via PGE2/EP2 signaling. *J. Exp. Med.* 206:61–68. http://dx.doi.org/10.1084/jem.20082058

Menendez, D., A. Inga, and M.A. Resnick. 2009. The expanding universe of p53 targets. *Nat. Rev. Cancer.* 9:724–737. http://dx.doi.org/10.1038/nrc2730

Mercer, J., N. Figg, V. Stoneman, D. Braganza, and M.R. Bennett. 2005. Endogenous p53 protects vascular smooth muscle cells from apoptosis and reduces atherosclerosis in ApoE knockout mice. *Circ. Res.* 96:667–674. http://dx.doi.org/10.1161/01.RES.0000161069.15577.ca

Merched, A.J., E. Williams, and L. Chan. 2003. Macrophage-specific p53 expression plays a crucial role in atherosclerosis development and plaque remodeling. *Arterioscler. Thromb. Vasc. Biol.* 23:1608–1614. http://dx.doi.org/10.1161/01.ATV.0000084825.88022.53

Merrick, B.A., S. Dhungana, J.G. Williams, J.J. Aloor, S. Peddada, K.B. Tomer, and M.B. Fessler. 2011. Proteomic profiling of S-acylated macrophage proteins identifies a role for palmitoylation in mitochondrial targeting of phospholipid scramblase 3. *Mol. Cell. Proteomics*. 10:M110.006007.

Moon, C., S. Kim, M. Wie, H. Kim, J. Cheong, J. Park, Y. Jee, N. Tanuma, Y. Matsumoto, and T. Shin. 2000. Increased expression of p53 and Bax in the spinal cords of rats with experimental autoimmune encephalomyelitis. *Neurosci. Lett.* 289:41–44. http://dx.doi.org/10.1016/S0304-3940(00)01253-2

Muñoz-Fontela, C., S. Macip, L. Martínez-Sobrido, L. Brown, J. Ashour, A. García-Sastre, S.W. Lee, and S.A. Aaronson. 2008. Transcriptional role of p53 in interferon-mediated antiviral immunity. *J. Exp. Med.* 205: 1929–1938. http://dx.doi.org/10.1084/jem.20080383

Newburger, D.E., and M.L. Bulyk. 2009. UniPROBE: an online database of protein binding microarray data on protein-DNA interactions. *Nucleic Acids Res.* 37:D77–D82. http://dx.doi.org/10.1093/nar/gkn660

Polyak, K., Y. Xia, J.L. Zweier, K.W. Kinzler, and B. Vogelstein. 1997. A model for p53-induced apoptosis. *Nature*. 389:300–305. http://dx.doi.org/10.1038/38525

Quinton, L.J., M.R. Jones, B.T. Simms, M.S. Kogan, B.E. Robson, S.J. Skerrett, and J.P. Mizgerd. 2007. Functions and regulation of NF-kappaB RelA during pneumococcal pneumonia. *J. Immunol.* 178:1896–1903.

Reeves, E.P., H. Lu, H.L. Jacobs, C.G. Messina, S. Bolsover, G. Gabella, E.O. Potma, A. Warley, J. Roes, and A.W. Segal. 2002. Killing activity of neutrophils is mediated through activation of proteases by K+ flux. *Nature*. 416:291–297. http://dx.doi.org/10.1038/416291a

Sablina, A.A., P.M. Chumakov, and B.P. Kopnin. 2003. Tumor suppressor p53 and its homologue p73alpha affect cell migration. *J. Biol. Chem.* 278:27362–27371. http://dx.doi.org/10.1074/jbc.M300547200

Sablina, A.A., A.V. Budanov, G.V. Ilyinskaya, L.S. Agapova, J.E. Kravchenko, and P.M. Chumakov. 2005. The antioxidant function of the p53 tumor suppressor. *Nat. Med.* 11:1306–1313. http://dx.doi.org/10.1038/nm1320

Sandelin, A., W. Alkema, P. Engström, W.W. Wasserman, and B. Lenhard. 2004. JASPAR: an open-access database for eukaryotic transcription factor binding profiles. *Nucleic Acids Res.* 32:D91–D94. http://dx.doi.org/10.1093/nar/gkh012

Siganaki, M., A.V. Koutsopoulos, E. Neofytou, E. Vlachaki, M. Psarrou, N. Soulitzis, N. Pentilas, S. Schiza, N.M. Siafakas, and E.G. Tzortzaki. 2010. Deregulation of apoptosis mediators' p53 and bcl2 in lung tissue of COPD patients. *Respir. Res.* 11:46. http://dx.doi.org/10.1186/1465-9921-11-46

Smeenk, L., S.J. van Heeringen, M. Koeppel, M.A. van Driel, S.J. Bartels, R.C. Akkers, S. Denissov, H.G. Stunnenberg, and M. Lohrum. 2008. Characterization of genome-wide p53-binding sites upon stress response. *Nucleic Acids Res.* 36:3639–3654. http://dx.doi.org/10.1093/nar/gkn232

Standish, A.J., and J.N. Weiser. 2009. Human neutrophils kill *Streptococcus pneumoniae* via serine proteases. *J. Immunol.* 183:2602–2609. http://dx.doi.org/10.4049/jimmunol.0900688

Suzuki, T., C. Yamashita, R.L. Zemans, N. Briones, A. Van Linden, and G.P. Downey. 2009. Leukocyte elastase induces lung epithelial apoptosis via a PAR-1-, NF-kappaB-, and p53-dependent pathway. *Am. J. Respir. Cell Mol. Biol.* 41:742–755. http://dx.doi.org/10.1165/rcmb.2008-0157OC

Takaoka, A., S. Hayakawa, H. Yanai, D. Stoiber, H. Negishi, H. Kikuchi, S. Sasaki, K. Imai, T. Shibue, K. Honda, and T. Taniguchi. 2003. Integration of interferon-alpha/beta signalling to p53 responses in tumour suppression and antiviral defence. *Nature*. 424:516–523. http://dx.doi.org/10.1038/nature01850

Tilley, S.L., M. Jaradat, C. Stapleton, D. Dixon, X. Hua, C.J. Erikson, J.G. McCaskill, K.D. Chason, G. Liao, L. Jania, et al. 2007. Retinoid-related orphan receptor gamma controls immunoglobulin production and Th1/Th2 cytokine balance in the adaptive immune response to allergen. *J. Immunol.* 178:3208–3218.

Tsai, W.C., R.M. Strieter, D.A. Zisman, J.M. Wilkowski, K.A. Bucknell, G.H. Chen, and T.J. Standiford. 1997. Nitric oxide is required for effective innate immunity against *Klebsiella pneumoniae*. *Infect. Immun.* 65: 1870–1875.

Turpin, E., K. Luke, J. Jones, T. Tumpey, K. Konan, and S. Schultz-Cherry. 2005. Influenza virus infection increases p53 activity: role of p53 in cell death and viral replication. *J. Virol.* 79:8802–8811. http://dx.doi.org/10.1128/JVI.79.14.8802-8811.2005

Valouev, A., D.S. Johnson, A. Sundquist, C. Medina, E. Anton, S. Batzoglou, R.M. Myers, and A. Sidow. 2008. Genome-wide analysis of transcription factor binding sites based on ChIP-Seq data. *Nat. Methods*. 5:829–834. http://dx.doi.org/10.1038/nmeth.1246

Vousden, K.H., and C. Prives. 2009. Blinded by the light: The growing complexity of p53. *Cell*. 137:413–431. http://dx.doi.org/10.1016/j.cell.2009.04.037

Wang, L., L. Bowman, Y. Lu, Y. Rojanasakul, R.R. Mercer, V. Castranova, and M. Ding. 2005. Essential role of p53 in silica-induced apoptosis. *Am. J. Physiol. Lung Cell. Mol. Physiol.* 288:L488–L496. http://dx.doi.org/10.1152/ajplung.00123.2003

Yun, Y.P., J.Y. Lee, E.K. Ahn, K.H. Lee, H.K. Yoon, and Y. Lim. 2009. Diesel exhaust particles induce apoptosis via p53 and Mdm2 in J774A.1 macrophage cell line. *Toxicol. In Vitro*. 23:21–28. http://dx.doi.org/10.1016/j.tiv.2008.09.018